Appl Phys A (2013) 112:839–845
DOI 10.1007/s00339-013-7577-7

Applied Physics A
Materials Science & Processing

Equation of state of $CaMnO_3$: a combined experimental and computational study

Wojciech Paszkowicz · Scott M. Woodley · Paweł Piszora · Bohdan Bojanowski · Jarosław Piętosa · Yngve Cerenius · Stefan Carlson · Christine Martin

Received: 9 June 2012 / Accepted: 19 January 2013 / Published online: 5 February 2013

Abstract Elastic properties of $CaMnO_3$ are of primary importance in the science and technology of $CaMnO_3$-based perovskites. From X-ray diffraction experiments performed at pressures up to 100 kbar using a diamond-anvil cell to hydrostatically compress our sample, a bulk modulus, K_0, of 1734(96) kbar was obtained after fitting parameters to the third-order Birch–Murnaghan equation of state. Mean field, semiclassical simulations predict, for the first time, the third-order equation-of-state parameters and show how the bulk modulus increases with pressure (the zero pressure value being 2062.1 kbar) and decreases with the extent of non-stoichiometry caused by the formation of oxygen vacancies. These trends are amplified for the shear modulus. A more accurate model that allows for the explicit reduction of Mn ions, or localization of excess electrons, yields qualitatively similar results. The experimental and calculated axial ratios show the same trends in their variation with rising pressure.

W. Paszkowicz (✉) · J. Piętosa
Institute of Physics, Polish Academy of Sciences, Lotnikow 32/46, 02-668 Warsaw, Poland
e-mail: paszk@ifpan.edu.pl

S.M. Woodley (✉)
Kathleen Lonsdale Materials Chemistry, Dept of Chemistry, University College London, 20 Gordon Str., London WC1H 0AJ, UK
e-mail: Scott.Woodley@ucl.ac.uk

P. Piszora
Dept of Materials Chemistry, Faculty of Chemistry, Adam Mickiewicz University, Grunwaldzka 6, 60-780 Poznań, Poland

B. Bojanowski
Institute of Physics, West Pomeranian University of Technology, al. Piastów 48, 70-311 Szczecin, Poland

Y. Cerenius · S. Carlson
MAX-Lab, Lund University, Box 118, 221 00 Lund, Sweden

C. Martin
Laboratoire CRISMAT-ENSICAEN (UMR CNRS 6805), CNRS, 6, bld Maréchal Juin, 14050 Caen Cedex 04, France

1 Introduction

ABO_3 perovskite oxides, (A = divalent alkaline-earth or trivalent rare-earth ion, B = transition metal ion) have been extensively studied in recent years. For materials of this class, physical properties are related to the occurrence of phenomena such as a Jahn–Teller distortion, a variation of the valence states of the transition metal ions, charge ordering, ionic conductivity, ferromagnetism, ferroelectricity, piezoelectricity, and the colossal magnetoresistance. Other phenomena such as a metal-to-insulator transition, magnetic-field-dependent structural transition, anomalous thermal conductivity temperature dependence or the isotopic effect on the Curie temperature, T_C, have also been reported for some materials of this class. Properties of perovskites are strongly pressure dependent. Pressure influences the transport properties; it can suppress the Jahn–Teller distortion and modify the conductivity type [1]. It changes the crucial structural quantities such as B–O bond lengths and B–O–B bond angles. The B–O–B bond angles influence the strength of double exchange interaction responsible for ferromagnetic coupling in Mn-containing perovskite oxides. In general, these bond angles have been found to increase under applied pressure, leading to an enhancement of the double exchange interactions and a rise of T_C (in the range up to 15–20 kbar) [2]; at larger pressures, the behavior is more complicated [3–5].

$CaMnO_3$ (orthorhombic, space group *Pnma*), a member of the ABO_3 family, is a parent compound for numerous multicomponent Mn-based perovskite oxides exhibiting colossal magnetoresistance, such as $La_{1-x}Ca_xMnO_3$ and

$Sr_{1-x}Ca_xMnO_3$. Mixed-valence manganites have the potential for applications based on their chemical and physical properties. Recently, doped $CaMnO_3$ has been considered as a material useful in thermoelectric power generation, in particular for waste heat recovery [6–8]. Elastic properties of $CaMnO_3$ under high pressure have not been rigorously studied up to now. The reported values of experimental and calculated equation-of-state (EOS) parameters, K_0, K', and V_0, exhibit large scatter. For example, the experimental value for K_0 is reported to be 528 kbar (as determined using ultrasonic measurements) [9], 1544(33) kbar (obtained by XRD at pseudohydrostatic conditions) [10], 1710 kbar (conditions close to hydrostatic in the whole pressure range studied) [11] and 2240(250) kbar (with hydrostatic conditions applied in a part of the fitting range) [12]. The importance of using hydrostatic compression and the suitability of pressure transmitting medium (PTM) formed from an alcohol-mixture for this purpose results from various recent experimental studies [13–15] (the hydrostaticity limit for this PTM is about 100 kbar). It is worth noting that for a related material, $SrMnO_3$, three experiments differing by measurement conditions led to large discrepancies in bulk-modulus value (see [16]; the authors briefly discuss some possible reasons and remedies).

Two EOS parameters (a_0 and K_0) have been reported in each of two theoretical approaches, DFT [17] and LMTO [18]. In three more recent simulations [9, 19, 20], only the bulk modulus has been calculated. In the cited papers, K_0 is predicted to be 675 kbar (Heterogeneous Metal Mixture model, HMM) [9], 1514.9 kbar and 2545.8 kbar (Modified Rigid Ion Model, MRIM) [20], 2114 kbar (Linear Muffin Tin Orbitals, LMTO) [18], 2150 kbar (Density Functional Theory, DFT) [17] and 3253.8 kbar (Born model) [19]. The discrepancies in both experimental and predicted values of bulk modulus are so large that the necessity of new investigation is evident; naturally the new experimental study must be performed at hydrostatic conditions within a possibly broad pressure range including the ambient pressure.

In this work, elastic properties of a stoichiometric $CaMnO_3$ sample are studied at high pressures. A p–V EOS is determined by fitting the diffraction data collected as a function of pressure. Furthermore, semi-classical simulations are employed in order to investigate the dependence of bulk modulus on pressure. Next, the discrepancies between the experimentally observed behavior and the theoretical predictions are discussed on the basis, in particular, of (demonstrated by simulations) trends taking place in the incorporation of oxygen vacancies.

2 Experimental

Our stoichiometric $CaMnO_3$ sample was synthesized in air in the form of a small bar at 1300 °C, starting from stoichiometric ratios of pure CaO and Mn_2O_3. The Ca:Mn ratio was controlled using X-ray energy-dispersive spectrometry (EDS) with accuracy of 0.02. As verified by measurements of the electric transport and magnetic properties, ideal oxygen stoichiometry was found and, moreover, the EDS of the cationic composition confirmed the cation homogeneity in the sample. The refined lattice parameters determined for the same sample (space group *Pnma*) are $a = 5.28159(4)$ Å, $b = 7.45730(4)$ Å, $c = 5.26748(4)$ Å, which gives $V = 207.467(4)$ [21].

The high-pressure diffraction experiments were performed using a membrane-driven diamond anvil cell (DXR-GM, EasyLab Technologies Ltd.), equipped with diamond anvils of 0.3 mm culet diameter. The sample was loaded into a hole (0.15 mm diameter, 0.1 mm depth) in the stainless-steel gasket placed in-between the diamonds. The data were collected at MAX-Lab (Lund, Sweden) I711 beamline [22] with wavelength of 0.91985 Å, using a MAR165 detector. The FIT2D program [23] was used for conversion of the 2D data to 1D. A 16:3:1 methanol-ethanol-water mixture [24] was used as the PTM. The small amount of sample in respect to the PTM volume was intentional, in order to minimize stresses connected with interaction between grains. The pressure was determined using laser-excited ruby luminescence. Lattice parameters were calculated from positions of nonoverlapping peaks using the UNITCELL program [25]. For $CaMnO_3$, the chosen approach for determination of lattice parameters from positions of nonoverlapping lines is appropriate for getting reliable lattice parameter values; to obtain a good accuracy, a synchrotron beam is used to ascertain good statistics, which is necessary because of the weak intensity of the peaks. The experimental Birch–Murnaghan (BM) EOS [26, 27] was fitted to 11 experimental $V(p)$ points below 100 kbar representing the hydrostatic range for the PTM applied, using the EOSFIT program [28, 29].

3 Theoretical approach

In our simulations, calculation of the lattice energy and physical properties for relaxed structures of various stoichiometries under a number of fixed pressures were performed using the General Utility Lattice Program (GULP) [30]; more details of our model including the interatomic potential parameters can be found in [21]. In fact, two mean-field approaches were employed to model the orthorhombic $CaMnO_{3-\delta}$ compounds. Reducing the occupancy of the oxygen sites to $(3-\delta)/3$ gives rise to an unphysical positive charge (for $\delta > 0$) on the unit cell. This charge is counterbalanced by either introducing a uniform neutralizing charge background ($-8\delta|e|$) across the unit cell or explicitly modeling a reduction of manganese by decreasing the mean

charge on the manganese sublattice from 4 to $(4 - 2\delta)|e|$. We will refer to these approaches as the "fixed" and "variable" charge models, respectively.

4 Results

4.1 Equation of state: experimental results

There is minimal noise in our experimental data for the unit cell size and volume, and axial ratio shown in Figs. 1 and 2 (points above 100 kbar which suffer from non-hydrostaticity are not shown). The present data $a = 5.283(1)$ Å, $b = 7.467(8)$ Å, $c = 5.267(1)$ Å, match well to the (mentioned in Sect. 2) ambient-pressure reference point determined for the same sample with a high accuracy. This agreement shows that, despite the difficulties due to high-pressure experiment setting and to the (specific for this material) strong peak overlap, the selected way of unit-cell size determination is appropriate. The obtained pressure dependence of lattice parameters is consistent with the results obtained using a different pressure medium (nitrogen) in Ref. [11] for pressures starting at 15.6 kbar; the data from Ref. [12] differ by a considerably higher scatter and larger absolute values of lattice parameters.

In the analysis of the experimental results, it is convenient to compare the (dimensionless) axial ratios. The present experiment shows a virtually constant value of $b/(a\sqrt{2})$ in the considered pressure range, whereas for c/a a slight tendency to increase from 0.9973 to 0.9987 is visible in Fig. 2. The slopes of all three experimental lines are apparently very small and almost identical. The (small) discrepancy in the absolute value of these lines, for both axial-ratios, can be due either to the difference in sample composition or to differences in lattice-parameter calculation methods. The marginal variation of axial ratios with pressure shows that the compression of $CaMnO_3$ is almost isotropic in the studied pressure range.

The obtained third-order BM EOS has the following parameters: $V_0 = 207.55(11)$ Å^3, $K_0 = 1734(96)$ kbar, $K' = 4.8(2.2)$ (fitting with second-order BM gave similar values $V_0 = 207.52(9)$ Å^3, $K_0 = 1767(28)$ kbar, K' being fixed at 4). Comparison with earlier data is not straightforward because of differences in experimental conditions as documented in Table 1 (different PTM and missing ambient pressure data for [11], pseudohydrostatic conditions for [10], and large scatter of experimental points for [12]). Moreover, the comparison of the present experimental data with the earlier ones may be affected by the fact that older datasets have been obtained assuming different EOS types and/or orders. The close agreement of the present value of experimental bulk modulus with that obtained using nitrogen as the PTM

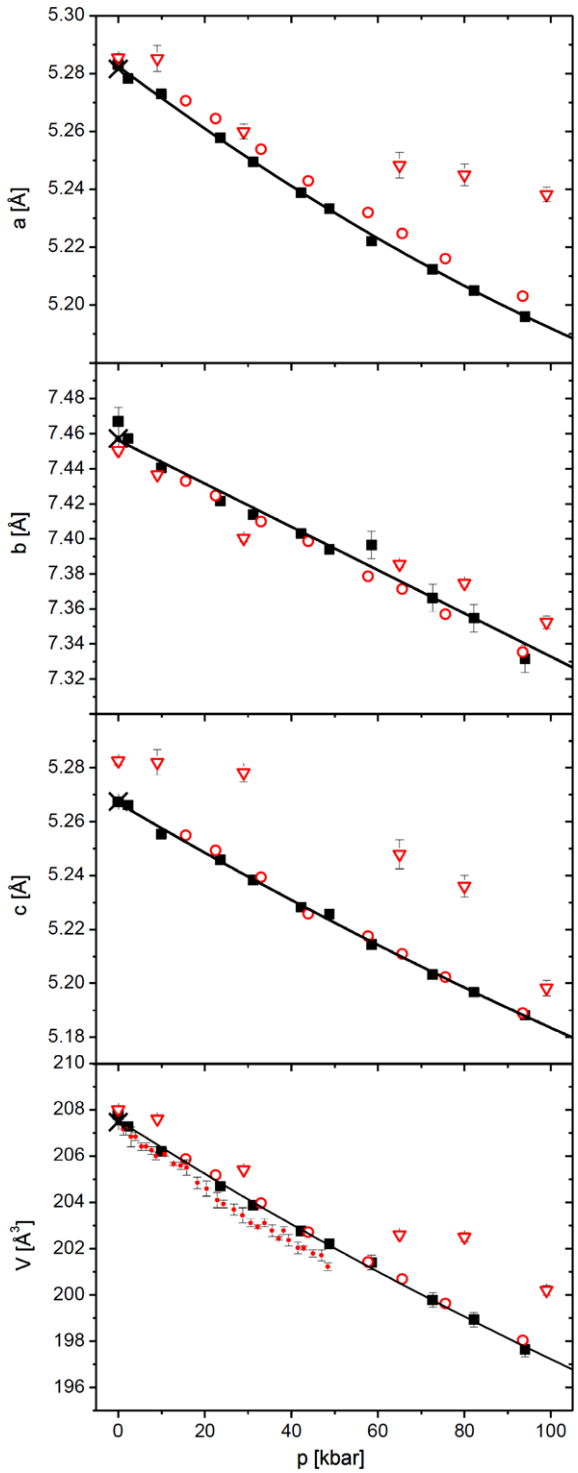

Fig. 1 Experimental pressure dependence of unit-cell parameters, a, b, c, and cell volume, V, for $CaMnO_3$. The symbols refer to: this work (■), [10] (points representing pseudohydrostatic experiment for the same sample), [11] (○), [12] (▽), and to a reference point at ambient pressure [21] (×). The *solid lines* for $a(p)$, $b(p)$, and $c(p)$ are guides to the eye; the *solid line* for $V(p)$ represents the third-order Birch—Murnaghan equation of state

for data collected over a broad pressure range within hydrostatic conditions [11] strongly suggests we have obtained reliable EOS parameters.

Interestingly, our experimental value for K_0 is (very) close to that reported for isostructural solid solutions with as high as 50 or 75 % occupation of the Ca site by a rare earth: $K_0 = 1860(50)$ or 2100 kbar for $La_{0.5}Ca_{0.5}MnO_3$ [11, 31], $K_0 = 1720(20)$ kbar for $Nd_{0.5}Ca_{0.5}MnO_3$ [32], and $K_0 = 1780$ kbar for $La_{0.75}Ca_{0.25}MnO_3$ [33]. However, for full La occupation, the bulk modulus value is strongly reduced to 1080(20) [1] or 1040 kbar [11], whereas for $PrMnO_3$ and $SmMnO_3$ larger values of 1639 and 1695 bar can be derived from [34] (the latter may be affected by non-hydrostatic compression conditions applied). More detailed analysis of such trends would require a dedicated study with identical experimental conditions applied.

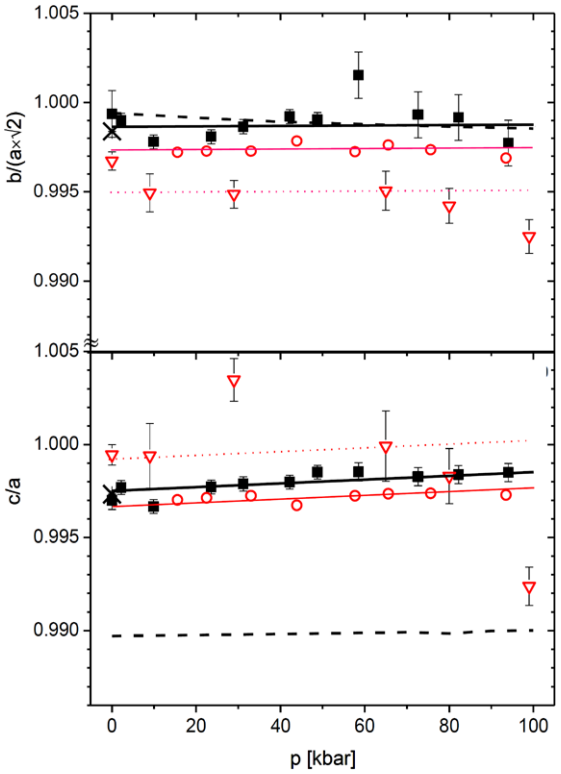

Fig. 2 Experimental and simulated pressure dependence of axial ratios, $b/(a\sqrt{2})$ (*top panel*) and c/a, for $CaMnO_3$ (*bottom panel*): experimental points (■) and *solid lines* as well as simulated dependencies (*dashed lines*) are displayed, Literature data are included for comparison from [11] (○, *thin solid lines*), [12] (▽, *thin dotted lines*), together with a reference point at ambient pressure [21] (×). All lines are guide-to-eye lines

4.2 Equation of state from simulations: results for stoichiometric case

The calculations yielded the pressure dependencies of simulated unit-cell volume (V), shear (S) and bulk (K) modulus for $CaMnO_3$ shown in Fig. 3; the axial ratios are displayed in Fig. 2. For each value of pressure, we ran our simulation twice, once with and then without *Pnma* symmetry imposed, and found similar V/V_0 curves as the symmetry of the fully relaxed crystal structure remains close to *Pnma* after energy minimization.

The pressure variation of unit-cell volume is accompanied by insignificant changes in the axial ratios: c/a increases by 0.0003, while $b/(a\sqrt{2})$ decreases by 0.0007, over 100 kbar. The following observations were made for the axial ratios, which are dimensionless and, therefore, are less dependent, than absolute values, on the exact fit of the potential parameters of our model; simulated data for $b/(a\sqrt{2})$ are in perfect agreement with the experimental ones, whereas the for c/a there is a small (less than 0.8 %) discrepancy, cf. Fig. 2. The slopes of the lines are only marginally different.

K appears to increase linearly with pressure, from 2062 to 2366 kbar (a 6 % change, which is smaller than that determined experimentally), while the rate of increase gradually drops for the shear modulus (S/S_0) at higher pressures.

Table 1 EOS parameters for $CaMnO_3$ as determined from fitting of experimental diffraction data [10–12] or other experiments

V_0 (Å^3)	K_0 (kbar)	K'	Experiment details			Assumed EOS type	Reference	Year
			Experimental method	PTM	Pressure range (kbar)			
207.5[a]	1710	5.9	ADXRD	nitrogen	15.6–386 (hr)	BM3	[11]	2003
208.39	528	–	ultrasonic	–	–	–	[9]	2008
208.0(1)	2240(25)	6.0(1.8)	ADXRD	AWM	0–365 (hlr)	M fit	[12]	2010
207.29(7)	1544(33)	4	EDXRD	pseudo-hydrostatic setting	0–48.4 (ph)	BM2	[10]	2011
207.55(11)	1734(96)	4.8(2.2)	ADXRD	AWM	0–100 (hr)	BM3	this work	2012

[a]Approximate value extracted from a graph included in Ref. [11] (exact value not reported). Abbreviations: ADXRD—angle dispersive X-ray diffraction, EDXRD—energy-dispersive X-ray diffraction, PTM—pressure transmitting medium, AWM—alcohol-water mixture, BMn fit—calculation with Birch-Murnaghan EOS of n-th order, M fit—calculation with Murnaghan EOS, hr—hydrostatic pressure in the fitting range, hlr—hydrostatic in a limited range of fitting (below about 100 kbar), ph—pseudohydrostatic

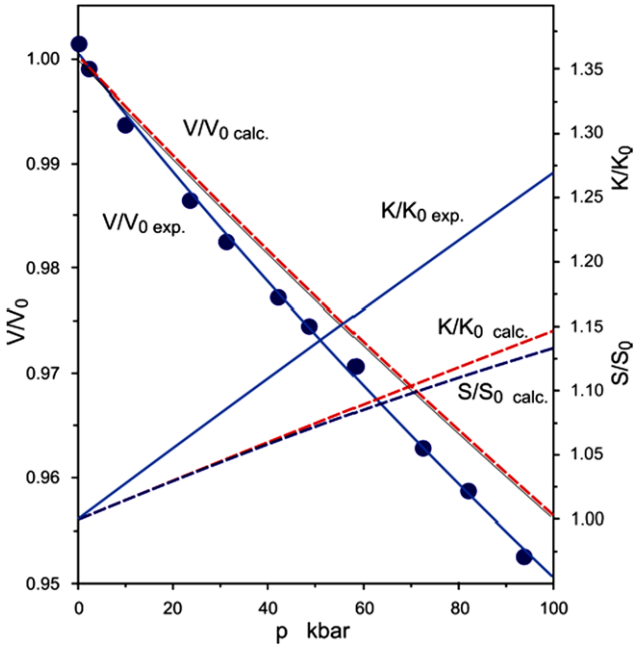

Fig. 3 Pressure dependence of unit-cell volume (V), shear (S), and bulk (K) modulus for $CaMnO_3$—as a ratio of zero pressure values. During simulations *Pnma* (various lines) or P_1 (*thin solid line* for V/V_0), symmetry was imposed. Experimental data: (*solid circles*) our work collected under hydrostatic compression and with an uncertainty of ± 1 kbar; (*blue line*) 2nd order BM EOS with $K_0 = 1776(37)$ kbar and $K' = 4$

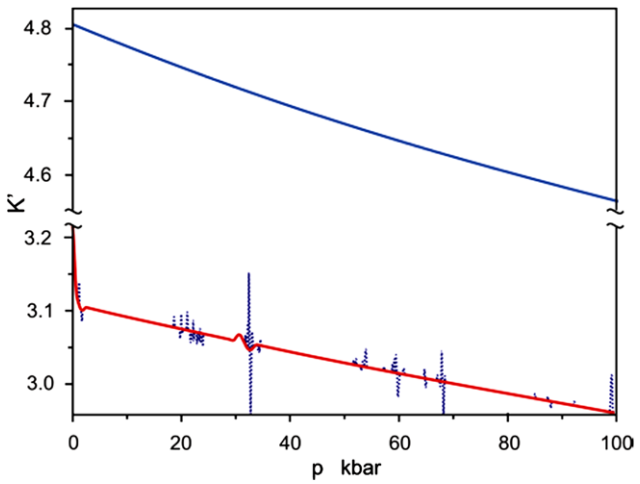

Fig. 4 Pressure dependence of bulk modulus derivative, K'. Experimental (*upper curve*) and simulated data are displayed. During simulations *Pnma* symmetry was imposed. Results for step size of 1 (*solid line*) and 0.2 (*dotted line*) kbar are compared

A more careful examination reveals that the rate of increase in K/K_0 also drops at higher pressures, which is more evident from the fact that K' decreases with increasing pressure (the noise visible in Fig. 4 is caused by premature completion during structural relaxations).

From our simulations of $CaMnO_3$, the lattice parameters (after minimizing the lattice enthalpy under ambient conditions) relaxed to 5.297 Å, 7.486 Å and 5.242 Å (giving $V_0 = 207.86$ Å^3). The remaining parameters of the equation of state have the values of 2062.1 kbar for the bulk modulus, and 3.3 and 3.1 for its first derivative, K_0' calculated numerically using a step size of 1 and 0.2 kbar, respectively. The obtained value of the shear modulus is 997.1 kbar, which is three times as large as the experimental value of 349 kbar reported in [9] and twice as large as compared to the room-temperature value (439 kbar) found for $Pr_{0.48}Ca_{0.52}MnO_3$ [35]. Note that the moduli are calculated from the elastic constants using Hill's definition [30].

The bulk moduli simulated using various approaches are compared in Table 2. Although higher than that obtained for our sample, the bulk modulus of $CaMnO_3$ in our simulations matches with the experiment much better than that obtained previously using a related approach [19] and compares well with those predicted by DFT (2150 kbar [17]) and the LMTO approach (2114 kbar [18]). The fact that three dissimilar theoretical approaches give similar K_0 values of about 330 kbar higher than that experimentally obtained for our sample (but lower than that reported for a different sample [12]) suggests that further investigation of the elastic properties of $CaMnO_3$ would be beneficial. We note that no target value for the bulk modulus was used during the refinement, or fit, of the potential parameters in our model, which was subsequently used here to investigate the qualitative behavior of physical properties with respect to pressure and stoichiometry.

4.3 Equation of state: theoretical results for non-stoichiometric case

We performed calculations for the nonstoichiometric compound, $CaMnO_{3-\delta}$, using the two different models described above. In both models, we assumed that there is no significant effect due to anion/vacancy ordering on the oxygen sites and that the effect of vacancies can be spread over all oxygen sites by averaging (which is described within the mean-field approach [30]).

Using the fixed-charge model, we find that the value for K_0 gradually softens as δ increases (see highest black curve in Fig. 5a) with $\Delta K_0(\delta = 0.3) = -137.4$ kbar, a trend which is repeated if pressure is increased, for example, at 40 and 100 kbar $\Delta K(\delta = 0.3) = -136.4$ and -135.1 kbar, respectively. The change in S_0 is much smaller for all pressures; for $\delta = 0.3$, $S_0 = 3.7$, $S_{40} = -0.9$, and $S_{100} = -10$ kbar, where the subscript indicates the respective pressures. The decrease of bulk modulus in oxygen-deficient tetragonal $La_{0.7}Sr_{0.3}MnO_{3-\delta}$ crystals is related to their lower atomic density [36], where experimentally $K_0 = 1080(50)$ kbar for $\delta = 0.15$ [36] and 1670 kbar for $\delta = 0$

Table 2 EOS parameters for $CaMnO_3$ as determined from present and earlier simulations

V_0 (Å^3)	K_0 (kbar)	K'	Simulation approach	Pressure range	Assumed EOS type	Reference	Year
210.94[a]	2150	–	DFT, primitive cubic cell assumed	–	–	[17]	1997
216.56[a]	2114	–	LMTO	–	–	[18]	1998
–	3253.8	–	Born model	–	–	[19]	2006
–	675	–	HMM	–	–	[9]	2008
–	1514.9 (LT)	–	MRIM	–	–	[20]	2009
–	2545.8 (HT)	–	MRIM	–	–	[20]	2009
207.86	2062.1	3.3 ($)	Born model	0–100	BM3	this work	2012

[a]Derived from the primitive cubic cell volume. Abbreviations: LT—low-temperature value, HT—high-temperature value (in paramagnetic state), ($) the value was 3.1 for calculations with a smaller pressure step. For abbreviations (DFT, LMTO, HMM, MRIM)—see the Introduction

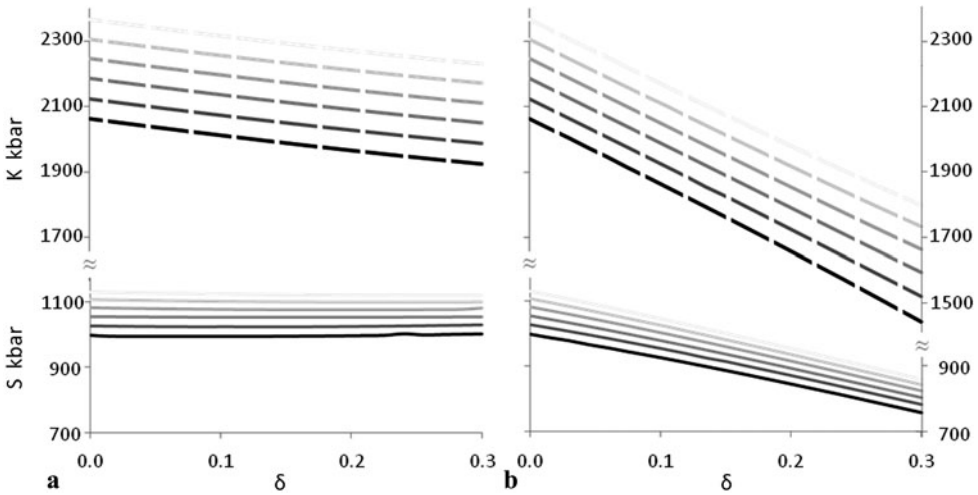

Fig. 5 The calculated bulk (*broken lines*) and shear (*solid lines*) modulus for $CaMnO_{3-\delta}$ using the fixed (**a**) and variable (**b**) charge models. Intensity of lines indicates the pressure; 0 (*black*), 20, 40, 60, 80, and 100 kbar

[37]—a much greater drop than that predicted for our system, $CaMnO_{3-\delta}$, using the assumption used in our first model that the additional charge resulting from oxygen vacancies is simply delocalized across the system.

In our simulations of the nonstoichiometric $CaMnO_{3-\delta}$, we expect an underestimation of the orthorhombicity of the structure, i.e., greater differences between lattice parameters as the tetragonal cell distorts to orthorhombic upon minimization of lattice energy, as the inclusion of vacancies would also create Jahn–Teller Mn^{3+} ions, which we have not explicitly included in our model. However, we can easily model a spread of an average charge on the manganese sites (the variable charge model), rather than use a neutralizing charge background, i.e., we now consider the effect of localization of the additional electrons on the Mn sublattice. From our simulations of $CaMnO_{2.7}$, we obtain $K_0 = 1445$, $S_0 = 758$, $K_{40} = 1596$, $S_{40} = 803$, $K_{100} = 1798$, and $S_{100} = 860$ kbar. Thus, the softening of both K and S with increasing δ is much quicker—compare Figs. 5a and 5b (note that simulations were performed for $\delta = 0.015n$, where n is an integer, $0, 1, 2 \ldots 20$). For $\delta = 0.03$ (close to the highest observed experimental δ value), the charge of the Mn shells is set to $3.94|e|$, as a consequence of which, the tilt of the octahedra increases (smaller Mn–O–Mn bond angles, which are now 156.52° and 157.61°), and K_0 has already softened to 2004 kbar and, therefore, agrees better with our observed value. We remind the reader that the bulk modulus obtained for our sample was not used in the fit of our interatomic potential parameters. To obtain a value of 1734(96) kbar, without refining potential parameters, we need δ to be as high as 0.14. Of course, although the statistical model may be somewhat "naïve," we can still ascertain the trend that oxygen vacancies will markedly reduce the value of K_0, while a decrease of the charge on the Mn sites leads to an increase of the tilt of the MnO_6 octahedra. As expected, the calculations indicate that for nonstoichiometric (i.e., less densely packed) material, the K_0 value is lower than for the stoichiometric compound.

5 Summary

In summary, high-pressure diffraction experiments for stoichiometric $CaMnO_3$ were undertaken in order to determine, for the first time, its equation of state (EOS) at hydrostatic conditions from a clean experimental volume/pressure dependence. In addition, semiclassical simulations were also performed in order to determined the simulated third-order third-order EOS. This investigation was completed in order to shed light on the discrepancies existing among the earlier reported experimental and theoretical bulk-modulus values. The experimental bulk modulus of $CaMnO_3$, derived by fitting the Birch–Murnaghan EOS to the $V_{\exp}(p)$ data, is 1734(96) kbar. The simulated value of 2062.1 is only slightly lower than those from previous DFT and LMTO calculations; the discrepancy between theory and experiment is only about 15 %. Our experiment and simulations show how the calculated bulk modulus increases with pressure. Moreover, from simulations, we predict how the bulk modulus decreases with the extent of nonstoichiometry resulting from the presence of oxygen vacancies—bulk modulus decreases with lower atomic density whether caused by internal (change in stoichiometry) or external pressure. Allowing for the explicit reduction of manganese ions, simulations produce qualitatively similar results, but with higher gradients, a trend that is amplified for the shear modulus.

Acknowledgements Professor C. Meneghini (Universita Roma Tre) is acknowledged for providing the unpublished data. The research leading to these results has received funding from both the European Community's Seventh Framework Programme (FP7/2007-2013), under grant agreement no. 226716, and EPSRC (EP/F067496).

References

1. I. Loa, P. Adler, A. Grzechnik, K. Syassen, U. Schwarz, M. Hanfland, G.K. Rozenberg, P. Gorodetsky, M.P. Pasternak, Phys. Rev. Lett. **87**, 125501 (2001)
2. V. Laukhin, J. Fontcuberta, J.L. García-Muñoz, X. Obradors, Phys. Rev. B **56**, R10009 (1997)
3. C. Cui, T.A. Tyson, Appl. Phys. Lett. **83**, 2856–2858 (2003)
4. C. Cui, T.A. Tyson, Z. Zhong, J.P. Carlo, Y. Qin, Phys. Rev. B **67**, 104107 (2003)
5. C. Cui, T.A. Tyson, Phys. Rev. B **70**, 94409 (2004)
6. M. Ohtaki, J. Ceram. Soc. Jpn. **119**(11), 770 (2011)
7. R. Funahashi, Sci. Adv. Mater. **3**, 682 (2011)
8. J.W. Fergus, J. Eur. Ceram. Soc. **32**, 525 (2012)
9. J.J.U. Buch, G. Lalitha, T.K. Pathak, N.H. Vasoya, V.K. Lakhani, P.V. Reddy, R. Kumar, K.B. Modi, J. Phys. D, Appl. Phys. **41**, 025406 (2008)
10. J. Piętosa, W. Paszkowicz, R. Minikayev, J. Nowak, C. Lathe, C. Martin, Powder Diffr. **26**, 262 (2011)
11. A. Sani, C. Meneghini, S. Mobilio, S. Ray, D.D. Sarma, J.A. Alonso, Exploring the high pressure phase diagram of $La_{1-x}Ca_xMnO_3$ (17 April 2003). arXiv:cond-mat/0304394v1
12. Y.-X. Liu, S. Qin, J.-Z. Jiang, K. Takumi, G.-H. Shi, Chin. Phys. C **34**(7), 1025 (2010)
13. R.J. Angel, M. Bujak, J. Zhao, G.D. Gatta, S.D. Jacobsen, J. Appl. Crystallogr. **40**, 26 (2007)
14. K. Takemura, J. Phys. Soc. Jpn. Suppl. A **76**, 202 (2007)
15. S. Klotz, J.-C. Chervin, P. Munsch, G. Le Marchand, J. Phys. D, Appl. Phys. **42**, 075413 (2009)
16. Y.-X. Liu, S. Qin, X.Wu.J.-Z. Jiang, T. Kikegawa, G.-H. Shi, Chin. Phys. C **35**, 514 (2011)
17. F. Freyria Fava, Ph. D'Arco, R. Orlando, R. Dovesi, J. Phys. Condens. Matter **9**, 489 (1997)
18. S.J. Youn, B.I. Min, J. Korean Phys. Soc. **32**, 576 (1998)
19. M.J. Akhtar, C.R.A. Catlow, B. Slater, A.M. Walker, S.M. Woodley, Chem. Mater. **18**, 1552 (2006)
20. A. Srivastava, N.K. Gaur, J. Magn. Magn. Mater. **321**(23), 3854 (2009)
21. W. Paszkowicz, J. Piętosa, S.M. Woodley, P.A. Dłużewski, M. Kozłowski, C. Martin, Powder Diffr. **25**, 46–59 (2010)
22. Y. Cerenius, K. Ståhl, L.A. Svensson, T. Ursby, Å. Oskarsson, J. Albertsson, A. Liljas, J. Synchrotron Radiat. **7**, 203–208 (2000)
23. A.P. Hammersley, S.O. Svensson, M. Hanfland, A.N. Fitch, D. Hausermann, High Press. Res. **14**, 235–248 (1996)
24. I. Fujishiro, G.J. Piermarini, S. Block, R.G. Munro, in *Proc. 8th AIRAPT Conference*, vol. II, ed. by C.M. Backman, T. Johannisson, L. Tegner, Uppsala, 17–22 August 1981, pp. 608–611
25. T.J.B. Holland, S.A.T. Redfern, Mineral. Mag. **61**, 65–77 (1997)
26. F. Birch, J. Geophys. Res. **83**(B3), 1257–1268 (1978)
27. R.M. Hazen, L.W. Finger, *Comparative Crystal Chemistry* (Wiley, Chichester, 1982)
28. R.J. Angel, in *Berichte aus Arbeitskreisen der DGK Nr. 9, VII. Workshop Powder Diffraction*, ed. by R.E. Dinnebier, Bayreuth, Oct. 4–8 2000 (Deutsche Gesellschaft für Kristallographie, Bayreuth, 2000), pp. 209–228
29. R. Angel, in *High-Pressure and High-Temperature Crystal Chemistry. MSA Reviews in Mineralogy and Geochemistry*, vol. 41, ed. by R.M. Hazen, R.T. Downs (Mineralogical Society of America, Washington, 2000), pp. 35–60
30. J.D. Gale, A.L. Rohl, Mol. Simul. **29**, 291–341 (2003)
31. D.P. Kozlenko, L.S. Dubrovinsky, I.N. Goncharenko, B.N. Savenko, V.I. Voronin, E.A. Kiselev, Phys. Rev. B **75**, 104408 (2007)
32. A. Arulraj, R.E. Dinnebier, S. Carlson, M. Hanfland, S. van Smaalen, Phys. Rev. Lett. **94**, 165504 (2005)
33. C. Meneghini, D. Levy, S. Mobilio, M. Ortolani, M. Nuñez-Reguero, A. Kumar, D.D. Sarma, Phys. Rev. B **65**, 012111 (2002)
34. J.-S. Zhou, J.B. Goodenough, Phys. Rev. B **68**, 054403 (2003)
35. M.A. Carpenter, C.J. Howard, R.E.A. McKnight, A. Migliori, J.B. Betts, V.R. Fanelli, Phys. Rev. B **82**, 134123 (2010)
36. D.P. Kozlenko, S.V. Trukhanov, E.V. Lukin, I.O. Troyanchuk, B.N. Savenko, Eur. Phys. J. B **58**, 361–365 (2007)
37. D.P. Kozlenko, I.N. Goncharenko, B.N. Savenko, V.I. Voronin, J. Phys. Condens. Matter **16**, 6755–6762 (2004)